

Four-fermion production in electron-positron collisions with NEXTCALIBUR

F. A. Berends

Instituut Lorentz, University of Leiden, P. O. Box 9506,
2300 RA Leiden, The Netherlands

C. G. Papadopoulos

Institute of Nuclear Physics, NCRS 'Democritos',
15310 Athens, Greece

and

R. Pittau

Dipartimento di Fisica Teorica, Università di Torino, Italy
INFN, Sezione di Torino, Italy

October 26, 2018

Abstract

We introduce a new, fully massive, Monte Carlo program to compute all four-fermion processes in e^+e^- collisions, including Higgs production. We outline our strategy for the matrix element evaluation, the phase space generation and the implementation of the leading higher order effects, and show, where available, comparisons with existing results.

Pacs: 11.15.-q, 13.10.-q, 13.38-b, 13.40,-f, 14.70.Fm

1 Introduction

Since the beginning of LEP2 four-fermion Physics underwent an extensive development. From an experimental point of view, new processes and effects, not included in the 1996 LEP2 Yellow Report [1], became relevant. All codes used so far have to be upgraded and extended with new features in order to match the improved experimental needs, especially in view of the final LEP2 analysis.

Although the needed improvements of the various event generators in use at LEP2 may differ from one code to another there often are three obvious steps to be taken, namely

- Including fermion masses, instead of neglecting them.
- Taking into account scale-dependent corrections and higher order contributions related to unstable particles.
- Improving the treatment of the QED radiation.

In the first place, fermion masses are relevant both for Higgs production and for single- W [2] or $\gamma\gamma$ dominated processes [3], when electrons are scattered in the very forward region.

Secondly, the correct scales have to be taken into account for processes dominated by quasi-real t -channel photons (single- W production) or s -channel photons with low virtuality ($Z\gamma^*$ processes), where tools adequate for studying high energy dominated processes, such as W^+W^- production, fail in describing the data.

Finally, it would be desirable to generate a realistic non-vanishing p_t distribution for the radiated photons.

These improvements should be made while, at the same time, the Monte Carlo program should be kept general enough to deal with all processes in all possible kinematical configurations. It is this requirement of having all processes and all kinematical configurations in one program, which is the challenge.

This paper paves the way to replace an existing code, EXCALIBUR [4], which describes all final states, by a new FORTRAN program, NEXTCALIBUR, which contains the above list of improvements. The demand of massive fermions leads us to a new type of matrix element calculation and severe

requirements on the phase space generation. This means in practice a new program, since the old program made essential use of massless fermions.

The structure of the work is as follows. In section 2, we describe the strategy for the massive matrix element evaluation and for the Monte Carlo integration in `NEXTCALIBUR`. In section 3 we present the treatment of the leading higher order contributions, mainly QED radiation and running of α_{QED} . Subsequently, in section 4, we show numbers and comparisons with other results in the literature. Finally, the last section is devoted to our conclusions.

2 The strategy

We solved the problem of the complexity in the massive matrix element evaluation by using `HELAC`, a `FORTTRAN` package for helicity amplitudes computation based on Dyson-Schwinger equations, as described in ref. [5], to which we refer for more details. Here we only point out that, in the case of massless particles, the algorithm is simplified from the beginning, by avoiding the computation of helicity amplitudes that are known to be zero. A very fast computation of the cross section can therefore be obtained. In table 1 we report comparisons in speed between `NEXTCALIBUR` (fully massive) and `EXCALIBUR` (massless) for three processes.

Process	<code>NEXTCALIBUR</code>	<code>EXCALIBUR</code>
$e^- \bar{\nu}_e \nu_e e^+$	34.6 (16)	12.3 (8)
$e^- \bar{\nu}_e u d$	35.0 (32)	5.4 (3)
$\mu^+ \mu^- b b$	62.0 (64)	6.1 (8)

Table 1: CPU time comparison between `NEXTCALIBUR` and `EXCALIBUR` in seconds/1000 points. In parenthesis we show the number of non vanishing helicity configurations. The speed difference is mainly due to the increased number of contributing helicities.

As for the phase space generation, we used the same multi-channel self-adjusting approach used in `EXCALIBUR`. Namely, we wrote a set of kinematical channels, each of them taking into account a different peaking structure of the integrand. The difference with the `EXCALIBUR` channels is that now all

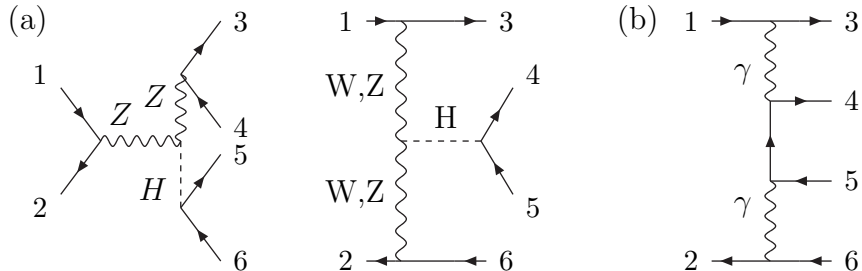


Fig 1: Higgs production (a) and double multi-peripheral (b) kinematical channels in NEXTCALIBUR.

fermion masses are taken into account. Furthermore the leading kinematical structures for Higgs production have been added (see fig. 1a).

More details can be found elsewhere [6]. We just mention here that the most complicated channel is the double multi-peripheral configuration given in fig. 1b, because three t -channel like singularities have to be mapped simultaneously: two of them due to quasi-real photons, and the third one induced by the fermion propagator.

3 Implementing higher order contributions

A first source of numerically important higher order contributions comes from the widths of the unstable bosons, that have to be included without breaking gauge invariance. Our approach is to use complex bosonic masses everywhere, also in the definition of the weak mixing angle. This obeys all relevant Ward Identities [7] and has been shown to be a very good approximation even in the forward region for t -channel dominated processes [8].

A second source of large higher order effects is the QED radiation. A very common solution is using the Structure Function formalism, namely a convolution of the Born cross section together with QED Initial State Radiators [9]. Such a strategy is implemented in most of the programs used for the analysis of the LEP2 data [10] and accurately reproduces the inclusive four-fermion cross sections, at least for s -channel dominated processes.

Recent studies have shown, by inspection with the soft limit of exact calculations, that the Structure Function formalism can still be used for t -

channel dominated processes, provided the scale q^2 of the radiators is chosen to be of the order of the virtuality of the exchanged t -channel photons. Our approach to the QED corrections is therefore using Initial State Structure Functions with a proper choice of q^2 for each of the two incoming legs ¹.

As to the scale q^2 , s should be taken for s -channel dominated processes, while, when a process is dominated by small t exchanges and $-t$ is much smaller than s , the scale is related to t . This is e.g. the case in small angle Bhabha scattering [11] and the proper scale is chosen as the one which reproduces roughly the exact first order QED correction, which is known for Bhabha scattering. A similar procedure now also exists for the multi-peripheral two photon process [12], since an exact first order calculation is also available [13]. In these t -channel dominated processes it is important to know whether a cross-section with angular cuts is wanted, since then the t -related scale will increase and the QED corrections as well. When no exact first order calculations are available the scale occurring in the first order soft corrections is also used as guideline to determine q^2 [12, 14].

In NEXTCALIBUR the choice of the scale is performed automatically by the program, event by event, according to the selected final state (see Table 2).

Final State	q_-^2	q_+^2
No e^\pm	s	s
1 e^-	$ t_- $	s
1 e^+	s	$ t_+ $
1 e^- and 1 e^+	$ t_- $	$ t_+ $
2 e^- and 2 e^+	$\min(t_-)$	$\min(t_+)$

Table 2: The choice of the QED scale in NEXTCALIBUR. q_\pm^2 are the scales of the incoming e^\pm while t_\pm represent the t -channel invariants obtained by combining initial and final state e^\pm momenta. When two combinations are possible, as in the last entry of the table, that one with the minimum value of $|t|$ is chosen, event by event.

However, as mentioned before, the choice of the appropriate q^2 is not the only required improvement to the treatment of the QED radiation. The

¹Presently, Final State radiation is neglected, but it can be included with analogous techniques.

increasing precision of the collected LEP2 data also requires the knowledge of the p_t spectrum of the emitted photons. We therefore use a particular form of p_t dependent Structure Functions [15], derived, at the first leading logarithmic order, for small values of p_t .

In practice, we replace the quantity

$$\ln\left(\frac{q^2}{m_e^2}\right) \quad \text{by} \quad \frac{1}{1 - c_i + 2\frac{m_e^2}{q^2}}$$

in the strictly collinear Structure Function for the i^{th} incoming particle, by explicitly generating c_1 and c_2 , the cosines (in the laboratory frame) of the emitted photons with respect to the incoming particles. Once $c_{1,2}$ are generated, together with the energy fractions $x_{1,2}$ and the azimuthal angles $\phi_{1,2}$, the momenta of two ISR photons are known. The four-fermion event is then generated in the c.m.s. of the incoming particles *after* QED radiation, and then boosted back to the laboratory frame.

We also take into account non leading terms with the substitution [16]

$$\ln\left(\frac{q^2}{m_e^2}\right) - 1 \quad \rightarrow \quad \frac{1}{1 - c_i + 2\frac{m_e^2}{q^2}} - 2\frac{m_e^2}{q^2} \frac{1}{(1 - c_i + 2\frac{m_e^2}{q^2})^2}.$$

The above choice ensures that the residue of the soft-photon pole gets proportional to $\ln(\frac{q^2}{m_e^2}) - 1$, after integration over c_i . The inclusive QED result is therefore exactly recovered, after integrating over the p_t spectrum and, at the same time, the pattern of the photon radiation is exact for small p_t values. Notice that the p_t spectrum is controlled by the same scale q^2 used in the strictly collinear Structure Functions, namely an s -channel scale for s -channel processes and a t -channel scale for t -channel dominated final states. The radiation pattern is therefore different in the two situations, as one naively expects. The presence of such a scale can also be thought as an extra handle to tune our Monte Carlo predictions to the data, to get a satisfactory description of the radiation.

Another problem, in presence of low t -channel scales, is that high energy renormalization schemes, such as the G_F scheme, fail in describing the data, because of the running of α_{QED} .

A possible solution is the Fermion-Loop approach of refs. [17]-[19], where all fermion corrections are consistently included by introducing running couplings $g(s)$ and $e(s)$ and re-summed bosonic propagators.

In presence of the $WW\gamma$ vertex, the above ingredients are not sufficient to ensure gauge invariance, because loop mediated vertices have to be consistently included. On the contrary, when no $WW\gamma$ vertex is present, the neutral gauge boson vertices, induced by the fermion loop contributions, are separately gauge invariant [18].

Instead of explicitly including the loop vertices, we follow a *Modified Fermion-Loop* approach. Namely, we neglect the separately gauge invariant neutral boson vertices, and include only the part of the $WW\gamma$ loop function necessary to renormalize the bare $WW\gamma$ vertex and to insure the $U(1)$ gauge invariance ². Our procedure is as follows. Besides running couplings, we use bosonic propagators

$$P_w^{\mu\nu}(s) = \left(s - M_w^2(s)\right)^{-1} \left(g_{\mu\nu} - \frac{p_\mu p_\nu}{M_w^2(s)}\right)$$

$$P_z^{\mu\nu}(s) = \left(s - M_z^2(s)\right)^{-1} \left(g_{\mu\nu} - \frac{p_\mu p_\nu}{M_z^2(s)}\right)$$

with running boson masses defined as

$$M_w^2(s) = \mu_w \frac{g^2(s)}{g^2(\mu_w)} - g^2(s)[T_W(s) - T_W(\mu_w)]$$

$$M_z^2(s) = \mu_z \frac{g^2(s)}{c_\theta^2(s)} \frac{c_\theta^2(\mu_z)}{g^2(\mu_z)} - \frac{g^2(s)}{c_\theta^2(s)} [T_Z(s) - T_Z(\mu_z)].$$

$T_{W,Z}(s)$ are contributions due to the top quark, $\mu_{w,z}$ the complex poles of the propagators (one can take, for instance, $\mu_{w,z} = M_{w,z}^2 - i\Gamma_{w,z}M_{w,z}$) and

$$s_\theta^2(s) = \frac{e^2(s)}{g^2(s)}, \quad c_\theta^2(s) = 1 - s_\theta^2(s).$$

The explicit form of the running functions $e^2(s)$, $g^2(s)$ and $T_{W,Z}(s)$ can be found in ref. [18].

The leading contributions are in the real part of the running couplings therefore we take only the real part of them. This also means that one can

²When using NEXTCALIBUR in this *running coupling mode*, $U(1)$ is preserved but $SU(2)$ is, in general, violated. The numerical effects of this are expected to be small at LEP2 energies. The implementation in the code of the fully $SU(2) \times U(1)$ gauge invariant solution of ref. [20] is under way.

replace, in the above formulae, $g^2(\mu_{w,z}) \rightarrow g^2(M_{w,z}^2)$, $c_\theta^2(\mu_z) \rightarrow c_\theta^2(M_z^2)$ and also $T_{W,Z}(\mu_{w,z}) \rightarrow T_{W,Z}(M_{w,z}^2)$.

When the $WW\gamma$ coupling is present, we introduce, in addition, the following effective three gauge boson vertex

$$\gamma_\mu \text{ wavy line } (p) \text{ --- } \text{dot} \text{ --- } \begin{matrix} p_+ \text{ wavy line } (W_\nu^+) \\ p_- \text{ wavy line } (W_\rho^-) \end{matrix} = i e(s) V_{\mu\nu\rho}$$

with $s = p^2$, $s^+ = p_+^2$, $s^- = p_-^2$ and

$$\begin{aligned} V_{\mu\nu\rho} &= g_{\mu\nu}(p - p_+)_\rho + g_{\nu\rho}(p_+ - p_-)_\mu (1 + \delta_V) + g_{\rho\mu}(p_- - p)_\nu \\ &+ \frac{(p_+ - p_-)_\mu}{s^- - s^+} \left[\left(\frac{g(s^-)}{g(s^+)} - 1 \right) p_{+\nu} p_{+\rho} - \left(\frac{g(s^+)}{g(s^-)} - 1 \right) p_{-\nu} p_{-\rho} \right] \\ \delta_V &= \frac{1}{g(s^+)g(s^-)(s^- - s^+)} \left[g^2(s^+)g^2(s^-) [T_W(s^-) - T_W(s^+)] \right. \\ &\left. + [g(s^+) - g(s^-)] [s^- g(s^+) + s^+ g(s^-)] \right]. \end{aligned} \quad (1)$$

It is the easy to see that, with the above choice for $V_{\mu\nu\rho}$, the $U(1)$ gauge invariance - namely current conservation - is preserved, even in presence of complex masses and running couplings, also with massive final state fermions.

From eq. (1), one deduces at least two effective ways to preserve $U(1)$. One can either compute $g(s)$ at a fixed scale (for example always with $s = M_W^2$), while keeping only the running of $e(s)$, or let all the couplings run at the proper scale. With the first choice the modification of the three gauge boson vertex is kept minimal (but the leading running effects included). With the second choice everything runs, but a heavier modification of the Feynman rules is required. At this point one should not forget that our approach is an effective one, the goodness of which can be judged only by comparing with the exact calculation of ref. [17]. We found that the second choice gives a better agreement for leptonic single- W final states, while the first one is closer to the exact result in the hadronic case, which is phenomenologically more relevant.

Therefore, we adopted this first option as our default implementation in NEXTCALIBUR.

We want to stress once more that the outlined solution is flexible enough to deal with any four-fermion final state, whenever small scales dominate. For example, once the given formulae are implemented in the Monte Carlo, the correct running of α_{QED} is taken into account also for s -channel processes as $Z\gamma^*$ production.

4 Numerical results

In tables 3 and 4, we show the total cross sections for the processes $e^+e^- \rightarrow e^+e^-\mu^+\mu^-$ and $e^+e^- \rightarrow e^+e^-e^+e^-$. Where available, we compare our predictions with the QED numbers published in ref. [3].

\sqrt{s}	BDK	NEXTCALIBUR
20	98.9 ± 0.6	99.20 ± 0.98
35	131.4 ± 2.2	131.03 ± 0.88
50	154.4 ± 0.9	152.33 ± 0.83
100	205.9 ± 1.2	204.17 ± 1.73
200	—	263.50 ± 1.31
200 (all)	—	265.58 ± 1.44

Table 3: σ_{tot} (in nb) for the process $e^+e^- \rightarrow e^+e^-\mu^+\mu^-$. Only QED diagrams, except in the last entry.

NEXTCALIBUR contains all electroweak diagrams, and can therefore be used to compute the electroweak background to the above $\gamma\gamma$ processes. By looking at the last entry of the tables, the latter is found to be less than 1 % at LEP2 energies, at least for totally inclusive quantities.

All numbers have been produced at the Born level, but ISR and running α_{QED} can be included as described in the previous section. Here we mainly want to demonstrate the ability of the program to cover all phase-space regions, without losing efficiency in the event generation.

At the moment, in order to get the necessary numerical accuracy, we run the program in quadruple precision. NEXTCALIBUR has been written in such a way that switching from double to quadruple precision simply implies adding

\sqrt{s}	BDK	NEXTCALIBUR
20	$0.920 \pm .011$	$0.905 \pm .011$
35	$1.070 \pm .015$	$1.079 \pm .014$
50	$1.233 \pm .018$	$1.214 \pm .016$
100	$1.459 \pm .025$	$1.485 \pm .020$
200	—	$1.776 \pm .019$
200 (all)	—	$1.787 \pm .030$

Table 4: σ_{tot} (in $nb \times 10^7$) for the process $e^+e^- \rightarrow e^+e^-e^+e^-$. Only QED diagrams, except in the last entry.

a flag at the compilation time. However, this option is really necessary only when two or more electrons are allowed in the very forward direction. For all the other kinematical configurations, with at most one electron lost in the beam pipe, double precision is sufficient. A version of the program using double precision in all possible situations is currently under study.

In tables 5, 6 and 7 we show, as a second example, single- W numbers produced with our Modified Fermion-Loop approach, as discussed in the previous section. Comparisons are made with the exact Fermion-Loop calculation of ref. [17]. The results of the complete Fermion-Loop are reproduced at 2% accuracy for both leptonic and hadronic single- W final states.

It should also be noted that, when neglecting Fermion-Loop corrections, one can directly compare NEXTCALIBUR with other massive Monte Carlo's and one finds excellent agreement for single- W production in the whole phase space [23].

In Figs. 2 and 3, we show, as an illustrative example, two distributions for the most energetic radiated photon in the processes $e^+e^- \rightarrow \mu^-\bar{\nu}_\mu u\bar{d}(\gamma)$, as predicted by NEXTCALIBUR. Only ISR photons are taken into account, $\sqrt{s} = 200$ GeV, $|\cos\theta_\mu| < 0.985$, $E_\mu > 5$ GeV and $M(u\bar{d}) > 10$ GeV. With the same set of events, by using as separation cuts for the emitted photons $E_\gamma > 1$ GeV and $|\cos\theta_\gamma| < 0.985$, we found the following values for the total, the non-radiative, the single-radiative (1 generated γ) and the double-radiative (2 generated γ 's) cross sections:

$$\begin{aligned} \sigma_{tot} &= 0.61727 \pm 0.0059 \text{ pb} & \sigma_{n-rad} &= 0.57819 \pm 0.0058 \text{ pb} \\ \sigma_{s-rad} &= 0.03854 \pm 0.0016 \text{ pb} & \sigma_{d-rad} &= 0.00054 \pm 0.0002 \text{ pb} \end{aligned}$$

$d\sigma/d\theta_e$	MFL	EFL	MFL/EFL - 1 (percent)
$0.0^\circ \div 0.1^\circ$	0.45062(70)	0.44784	+0.62
$0.1^\circ \div 0.2^\circ$	0.06636(28)	0.06605	+0.47
$0.2^\circ \div 0.3^\circ$	0.03848(21)	0.03860	-0.31
$0.3^\circ \div 0.4^\circ$	0.02726(18)	0.02736	-0.37
σ_{tot}	83.26(9)	83.28(6)	-0.02

Table 5: $d\sigma/d\theta_e$ [pb/degrees] and σ_{tot} [fb] for the process $e^+e^- \rightarrow e^-\bar{\nu}_e u\bar{d}$. The first column is our Modified Fermion-Loop, the second one is the exact Fermion-Loop of ref. [17]. $\sqrt{s} = 183$ GeV, $|\cos\theta_e| > 0.997$, $M(u\bar{d}) > 45$ GeV. QED radiation not included. The number in parenthesis shows, when available, the integration error on the last digits.

$d\sigma/d\theta_e$	MFL	EFL	MFL/EFL - 1 (percent)
$0.0^\circ \div 0.1^\circ$	0.13218(26)	0.13448	-1.7
$0.1^\circ \div 0.2^\circ$	0.01997(10)	0.02031	-1.7
$0.2^\circ \div 0.3^\circ$	0.01171(8)	0.01194	-1.9
$0.3^\circ \div 0.4^\circ$	0.00838(6)	0.00851	-1.5
σ_{tot}	25.01(3)	25.53(4)	-2.0

Table 6: $d\sigma/d\theta_e$ [pb/degrees] and σ_{tot} [fb] for the process $e^+e^- \rightarrow e^-\bar{\nu}_e\nu_\mu\mu^+$. The first column is our Modified Fermion-Loop, the second one is the exact Fermion-Loop of ref. [17]. $\sqrt{s} = 183$ GeV, $|\cos\theta_e| > 0.997$, $|\cos\theta_\mu| < 0.95$ and $E_\mu > 15$ GeV. QED radiation not included. The number in parenthesis shows, when available, the integration error on the last digits.

$d\sigma/d\theta_e$	MFL	EFL	MFL/EFL - 1 (percent)
$0.0^\circ \div 0.1^\circ$	0.62694(98)	0.62357	+0.54
$0.1^\circ \div 0.2^\circ$	0.08850(38)	0.08798	+0.59
$0.2^\circ \div 0.3^\circ$	0.05100(30)	0.05141	-0.80
$0.3^\circ \div 0.4^\circ$	0.03672(25)	0.03646	+0.71
σ_{tot}	113.73 (13)	113.67(8)	+0.05

Table 7: $d\sigma/d\theta_e$ [pb/degrees] and σ_{tot} [fb] for the process $e^+e^- \rightarrow e^-\bar{\nu}_e u\bar{d}$. The first column is our Modified Fermion-Loop, the second one is the exact Fermion-Loop of ref. [17]. $\sqrt{s} = 200$ GeV, $|\cos\theta_e| > 0.997$, $M(u\bar{d}) > 45$ GeV. QED radiation not included. The number in parenthesis shows, when available, the integration error on the last digits.

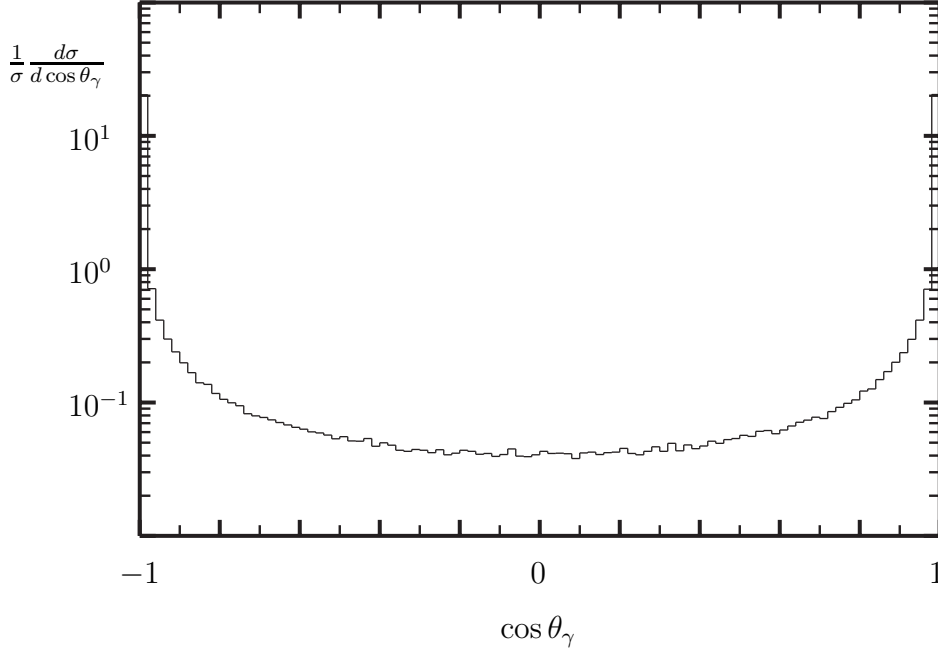


Fig 2: $\cos\theta_\gamma$ distribution (with respect to the incoming e^+) for the most energetic photon in the process $e^+e^- \rightarrow \mu^-\bar{\nu}_\mu u\bar{d}(\gamma)$.

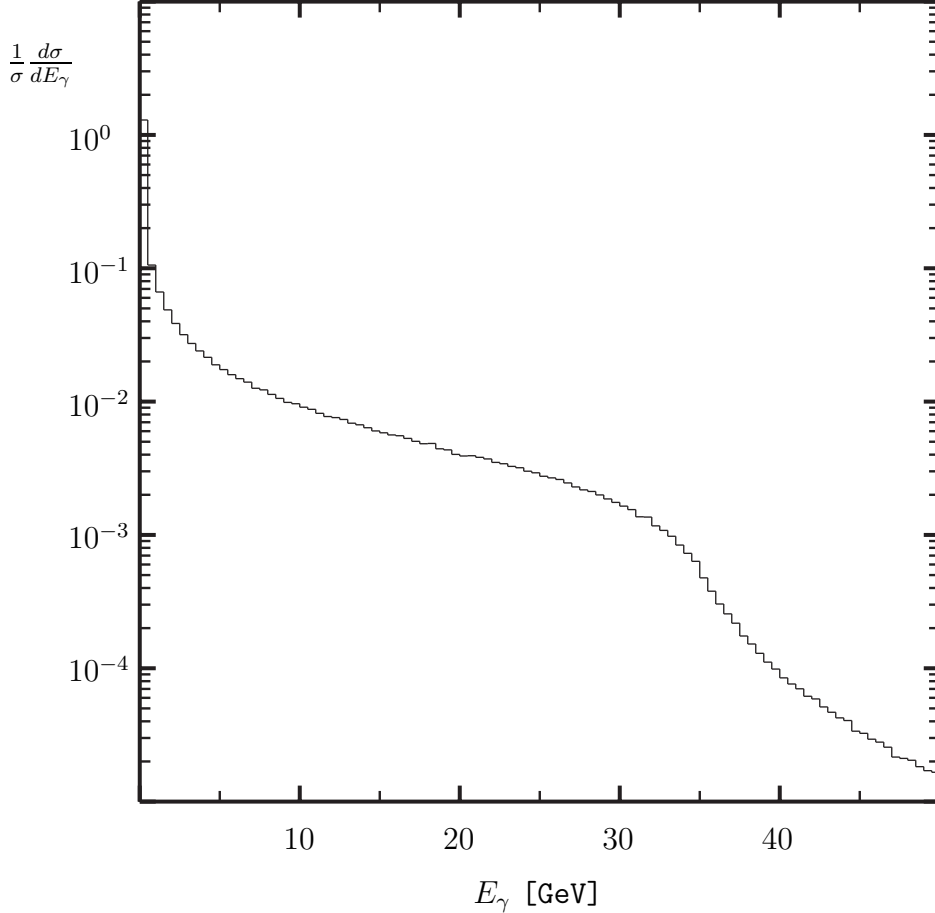


Fig 3: E_γ distribution for the most energetic photon in the process $e^+e^- \rightarrow \mu^- \bar{\nu}_\mu u \bar{d}(\gamma)$.

Finally, in tables 8 and 9, we show comparisons with the Higgs cross sections published in ref. [21], by choosing WPHACT [22] as a benchmark program. We devoted special care to implement exactly the same input parameters of ref. [21]. For completeness we list them here:

- Standard LEP2 input parameter set (see ref. [1]).
- Massless fermions everywhere, except in the Higgs coupling to the b .
- Running widths in the bosonic propagators.

m_H (GeV)	65	90	115
Final state	$\mu^+\mu^-bb$		
WPHACT	32.7141(68)	1.59946(64)	1.05953(56)
NEXTCALIBUR	32.691(19)	1.5999(18)	1.0588(11)
Final state	$\nu_\mu\bar{\nu}_\mu bb$		
WPHACT	64.238(14)	2.3661(10)	1.29237(82)
NEXTCALIBUR	64.256(35)	2.3651(27)	1.2910(14)
Final state	$\nu_e\bar{\nu}_e bb$		
WPHACT	71.694(27)	5.0996(23)	1.08027(89)
NEXTCALIBUR	71.778(84)	5.086(12)	1.0776(13)

Table 8: Cross sections, in fb, for Higgs production at $\sqrt{s} = 175$ GeV. See text for the input parameters.

- $\Gamma_H = \frac{\alpha m_H}{8 M_W^2 \sin^2 \theta_W} (m_\tau^2 + 3m_b^2 + 3m_c^2)$.
- $m_\tau = 1.777$ GeV, $m_b = 2.9$ GeV and $m_c = 0.75$ GeV.
- No ISR, no QCD corrections but all background diagrams included.
- $M_Z - 25$ GeV $\leq m_{\ell\bar{\ell}} \leq M_Z + 25$ GeV and $m_{b\bar{b}} \geq 50$ GeV.

It is worth mentioning explicitly that NEXTCALIBUR can consistently include fermion masses everywhere, and that they have been neglected in the presented numbers just for the sake of comparison.

5 Conclusions

We introduced NEXTCALIBUR, a new Monte Carlo program to study four-fermion processes in e^+e^- collisions. We outlined our strategy for including Higgs, fermion masses and leading higher order effects, without losing efficiency in the event generation. The program is meant to upgrade the performances of an already existing code [4].

We concentrated mainly on QED and scale-dependent corrections, without making any attempt to include genuine weak contributions. While the

m_H (GeV)	65	90	115
Final state	$\mu^+\mu^-bb$		
WPHACT	37.3990(64)	24.4727(40)	10.7027(24)
NEXTCALIBUR	37.394(21)	24.471(14)	10.7006(77)
Final state	$\nu_\mu\bar{\nu}_\mu bb$		
WPHACT	72.927(16)	47.222(12)	19.841(11)
NEXTCALIBUR	72.929(46)	47.231(33)	19.842(19)
Final state	$\nu_e\bar{\nu}_e bb$		
WPHACT	80.611(34)	53.335(19)	20.893(12)
NEXTCALIBUR	80.507(96)	53.280(67)	20.897(24)

Table 9: Cross sections, in fb, for Higgs production at $\sqrt{s} = 192$ GeV. See text for the input parameters.

latter are certainly relevant for LEP2 precision measurements, such as σ_{WW} and M_W , they do not seem to be necessary for all the other observables. In that respect NEXTCALIBUR represents a solid tool for the final analysis of the LEP2 four-fermion data and for studying e^+e^- Physics in general.

In the near future, two big improvements of the program are foreseen. First of all the inclusion in the matrix element of anomalous couplings. Secondly, the implementation of the formalism of ref. [20] to incorporate running couplings and finite boson widths effects without breaking $SU(2) \times U(1)$ gauge invariance.

Notice that, given our computational strategy, the only needed modification is the insertion of additional Feynman rules in the matrix element, all the rest remaining the same. Therefore, we do not expect difficulties of principle in the actual implementation.

Acknowledgements

Fruitful discussions with all the participants in the CERN LEP2 Monte Carlo Workshop [23] are acknowledged, in particular with Giampiero Passarino and Alessandro Ballestrero.

References

- [1] D. Bardin et al., in Physics at LEP2, CERN 96-01 (1996), eds. G. Altarelli, T. Sjöstrand and F. Zwirner, Vol 2, p. 3.
- [2] E. Boos and M. Dubinin, hep-ph/9909214;
G. Passarino, hep-ph/9810416;
M. A. Doncheski, S. Godfrey and K. A. Peterson, hep-ph/9710299;
T. Tsukamoto, Acta Phys. Polon. **B28**, 695 (1997);
T. Tsukamoto and Y. Kurihara, Phys. Lett. **B389**, 162 (1996);
K. Huitu, J. Maalampi and M. Raidal, hep-ph/9602387;
C. G. Papadopoulos, Phys. Lett. **B333**, 202 (1994);
C. G. Papadopoulos, in Muenchen/Annecy/Hamburg 1992-93, e^+e^- collisions at 500-GeV, pt. C 199-205.
- [3] F. A. Berends, P. H. Daverveldt and R. Kleiss, Phys. Lett. **B148**, 489 (1984) and Nucl. Phys. **B253**, 441 (1985).
- [4] F. A. Berends, R. Pittau and R. Kleiss, Comput. Phys. Commun. **85**, 437 (1995) and Nucl. Phys. **B424**, 308 (1994).
- [5] A. Kanaki and C. G. Papadopoulos, hep-ph/0002082.
- [6] F. A. Berends, C. G. Papadopoulos and R. Pittau, in preparation.
- [7] A. Denner, S. Dittmaier, M. Roth and D. Wackerth, Nucl. Phys. **B560**, 33 (1999).
- [8] E. Accomando, A. Ballestrero and E. Maina, hep-ph/9911489.
- [9] E. A. Kuraev and V. S. Fadin, Yad. Fiz. **41**, 753 (1985) [Sov. J. Nucl. Phys. **41**, 466 (1985)];
G. Altarelli and G. Martinelli, in Physics at LEP, CERN-Yellow Report 86-06, eds. J. Ellis and R. Peccei (CERN, Geneva, February 1986);
O. Nicrosini and L. Trentadue, Phys. Lett. **B196**, 551 (1987);
F. A. Berends, G. Burgers and W. L. van Neerven, Nucl. Phys. **B297**, 429 (1988) and **B304**, 921E (1988).
- [10] See, for example, F. A. Berends, R. Pittau and R. Kleiss, Nucl. Phys. **B426**, 344 (1994).

- [11] W. Beenakker, F. A. Berends and S. C. van der Marck, Nucl. Phys. **B349**, 323 (1991).
- [12] Y. Kurihara, J. Fujimoto, Y. Shimizu, K. Kato, K. Tobimatsu and T. Munehisa, hep-ph/9912520.
- [13] F. A. Berends, P. H. Daverveldt and R. Kleiss, Nucl. Phys. **B253**, 421 (1985).
- [14] G. Montagna, M. Moretti, O. Nicrosini, A. Pallavicini and F. Piccinini, paper in preparation and in *On photon radiation in single-W process*, talk at the LEP2 Monte Carlo Workshop [23], Oct. 12 1999.
- [15] G. Montagna, M. Moretti, O. Nicrosini and F. Piccinini, Nucl. Phys. **B541**, 31 (1999);
O. Nicrosini and L. Trentadue, Nucl. Phys. **B318**, 1 (1989) and Phys. Lett. **B231**, 487 (1989).
- [16] F. A. Berends and R. Kleiss, Nucl. Phys. **B260**, 32 (1985) and **B178**, 141 (1981).
- [17] G. Passarino, hep-ph/0001212 and hep-ph/9911482.
- [18] W. Beenakker et al., Nucl. Phys. **B500**, 255 (1997).
- [19] E. Argyres et al., Phys. Lett. **B358**, 339 (1995).
- [20] W. Beenakker, F. A. Berends and A. P. Chapovsky, hep-ph/9909472.
- [21] M. L. Mangano et al., in Physics at LEP2, CERN 96-01 (1996), eds. G. Altarelli, T. Sjöstrand and F. Zwirner, Vol 2, p. 299.
- [22] E. Accomando and A. Ballestrero, Comput. Phys. Commun. **99**, 270 (1997).
- [23] <http://www.to.infn.it/~giampier/lep2.html>.